RSC Advances

PAPER

View Article Online
View Journal | View Issue

Cite this: *RSC Adv.*, 2016, **6**, 106109

Published on 01 November 2016. Downloaded by Bilkent University on 12/23/2018 6:13:57 PM.

Nanoscale selective area atomic layer deposition of TiO_2 using e-beam patterned polymers†

Ali Haider,[ab] Mehmet Yilmaz,[b] Petro Deminskyi,[b] Hamit Eren[ab] and Necmi Biyikli*[c]

Here, we report nano-patterning of TiO_2 *via* area selective atomic layer deposition (AS-ALD) using an e-beam patterned growth inhibition polymer. Poly(methylmethacrylate) (PMMA), polyvinylpyrrolidone (PVP), and octafluorocyclobutane (C_4F_8) were the polymeric materials studied where PMMA and PVP were deposited using spin coating and C_4F_8 was grown using inductively coupled plasma (ICP) polymerization. TiO_2 was grown at 150 °C using tetrakis(dimethylamido) titanium (TDMAT) and H_2O as titanium and oxygen precursors, respectively. Contact angle, scanning electron microscopy (SEM), spectroscopic ellipsometry, and X-ray photoelectron spectroscopy (XPS) measurements were performed to investigate the blocking/inhibition effectiveness of polymer layers for AS-ALD of TiO_2. TiO_2 was grown with different numbers of growth cycles (maximum = 1200 cycles) on PMMA, PVP, and C_4F_8 coated substrates, where PMMA revealed complete growth inhibition up to the maximum number of growth cycles. On the other hand, PVP was able to block TiO_2 growth up to 300 growth cycles only, whereas C_4F_8 showed no TiO_2-growth blocking capability. Finally, mm-, μm-, and nm-scale patterned selective deposition of TiO_2 was demonstrated exploiting a PMMA masking layer that has been patterned using e-beam lithography. SEM, energy-dispersive X-ray spectroscopy (EDX) line scan, EDX elemental mapping, and XPS line scan measurements cumulatively confirmed the self-aligned deposition of TiO_2 features. The results presented for the first time demonstrate the feasibility of achieving self-aligned TiO_2 deposition *via* TDMAT/H_2O precursor combination and e-beam patterned PMMA blocking layers with a complete inhibition for >50 nm-thick films.

Received 26th September 2016
Accepted 28th October 2016

DOI: 10.1039/c6ra23923d

www.rsc.org/advances

Introduction

Atomic layer deposition (ALD) is a vapor phase deposition scheme that enables the conformal coating of thin films with sub-nanometer thickness control. In contrast to standard physical and/or chemical vapor deposition techniques, an ALD process relies on alternating pulses of gaseous precursors separated by purge steps. During each precursor exposure, surface reactions occurring only at the reactive sites restrict the film growth to a sub-monolayer within a unit ALD cycle. Due to the evacuation/purge process of unreacted precursor molecules and reaction byproducts after each precursor exposure, influence of uncontrolled parameters (*e.g.*, randomness of the precursor flux and hard-to-control gas-phase reactions) is considerably suppressed. This self-limiting characteristic of ALD offers precise thickness control at sub-angstrom level with a superior conformality and uniformity over large areas, arbitrary topography, and complex structures.[1–3]

Controlling the lateral dimensions of thin films by patterning is pivotal in microelectronics industry due to ever-increasing trend towards further miniaturization of device feature sizes.[4,5] Conventionally, thin film patterning is achieved by photolithography which includes several processing steps such as resist spinning, UV exposure, resist development, and film etching. ALD processes, in which film nucleation critically relies on the surface chemistry between gaseous precursors and the solid surface, provide an attractive opportunity for performing area-selective deposition by chemically modifying the substrate surface. Local modification of substrate surface opens up possibilities to achieve lateral control over film growth in addition to robust thickness control during ALD process.[6–11] Area-selective ALD (AS-ALD) might pave the way for low-temperature self-aligned nanoscale device fabrication by reducing or eliminating lithography/etch process steps and minimizing hazardous reagent use. Taking these significant advantages into consideration, the efforts of developing reliable and effective AS-ALD recipes have attracted considerable interest in recent years. ALD-enabled nano-patterning has been classified under two broad categories, one with area-activated agents and the other with area-deactivated blocking/inhibition

[a]Institute of Materials Science and Nanotechnology, Bilkent University, Ankara 06800, Turkey

[b]UNAM – National Nanotechnology Research Center, Bilkent University, Ankara 06800, Turkey

[c]Electrical and Computer Engineering Department, Utah State University, Logan, UT 84322, USA. E-mail: n.biyikli@aggiemail.usu.edu

† Electronic supplementary information (ESI) available. See DOI: 10.1039/c6ra23923d

Published on 01 November 2016. Downloaded by Bilkent University on 12/23/2018 6:13:57 PM.

layers.[7,9–34] So far, majority of the AS-ALD studies have been performed using area-deactivated approach where mostly self-assembled monolayers (SAMs) are utilized as the growth-blocking layers by covering the chemically reactive sites on the substrate and exposing non-reactive groups.[7,9,23,27,29–40] Alkyl silanes *e.g.*, alkyl trichlorosilanes, alkyl triethoxysilanes, *etc.* have been exploited as mono-layered surface modifiers to block ALD nucleation of various metal oxide thin films and metallic nanoparticles/thin films.[10,13,36,37,41–48] In this strategy, chlorosilane compounds chemically react with hydroxyl sites on the substrate surface and expose only unreactive alkyl groups on the surface which serve as effective ALD nucleation preventing agents. Although promising, this approach depends critically on the availability of defect-free SAM blocking layers, otherwise the defects in SAM act as nucleation centers leading to reduced selectivity and eventually non-selective growth. Moreover, preparing defect-free SAMs is not easy and generally takes extremely long synthesis times (up to 48 h).[23,31,41,48] Even with a decent quality SAM coating, growth selectivity might still be limited to a few nanometers of film thickness. In addition, patterning of SAMs has generally been attained using non-standard lithographic techniques such as micro-contact printing which further makes it a laborious task to obtain defect-free SAMs. Such a slow and rather unreliable masking process may undermine the capability of AS-ALD process as a straight-forward, fast, and reliable technique for potential use in high-volume manufacturing.

Overcoming the limitations associated with SAM-based mask layers require the production of easily patterned, non-reactive, and defect-free blocking layer materials. Polymer films present an alternative way to prepare defect free masking layers which physically screen the active sites on the substrate and enable AS-ALD process.[24,49–51] Indeed, polymer films with several critical advantages including quick and easy coating, defect free film quality, and ease of patterning have been implemented in majority of the lithographic patterning processes. In this scenario, if one can identify a polymer or a group of polymers that are unreactive towards ALD precursors which can also be easily patterned and removed after the growth, then that polymer film can be potentially used as a blocking layer to achieve AS-ALD process. Such a self-aligned AS-ALD approach to obtain a directly patterned structure of a desired ALD film may avoid additional etching and lift-off processes associated with regular lithography-based patterning methods.

AS-ALD of TiO_2, CeO_2, ZnO, N-doped ZnO, Ru, Rh, and Pt have been demonstrated using various polymer layers as growth inhibitor.[24,25,31,49–54] ALD-grown films might start nucleating on the polymer blocking layer after a certain number of ALD-cycles; patterning of such films are demonstrated *via* conventional lift-off processes. Al_2O_3, TiO_2, ZnO, ZrO_2, HfO_2, CeO_2, and Co have been patterned using polymer layers as lift-off resist films.[55–59] In most of these studies poly(methyl methacrylate) (PMMA) or polyvinylpyrrolidone (PVP) have been utilized as either blocking or lift-off layers. Both polymers feature ease in coating, compatibility with conventional patterning techniques, and rather simple removal after the growth. Recently PMMA has also been utilized as a chemical sponge in sequential infiltration synthesis (SIS) technique to achieve AS-ALD of Al_2O_3.[60]

Blocking capability for area-selective deposition might depend not only on the type of blocking polymer materials used, but also on the specific ALD process conditions (growth recipes) such as employed precursors and doses, unit cycle and cumulative process time, reactor pressure, substrate temperature, *etc.*[11,61] AS-ALD of TiO_2 layers have been carried out previously using PMMA as blocking layer with titanium tetrachloride ($TiCl_4$), titaniumisopropoxide $Ti(O^iPr)_4$, and titaniumethoxide $Ti(OMe)_4$ as titanium precursor sources.[24,25,53,59] Among these studies, successful AS-ALD results were achieved using $Ti(O^iPr)_4$ and $Ti(OMe)_4$ precursors, both exhibiting effective growth inhibition on PMMA surfaces. On the other hand, TiO_2 growth was observed on PMMA for $TiCl_4$ precursor and therefore, patterning was performed using routine lift-off method. Thin film patterning of TiO_2 in these studies was accomplished on a μm PMMA pattern defined using either optical or thermal probe based lithography methods. However, with the continuous downward scaling of electronic devices, self-aligned area selective ALD using a nano patterning scheme such as e-beam lithography is highly imperative. Adoption of selective deposition approaches in device fabrication also requires those thin film growth precursors which are completely unreactive towards growth inhibition layers in order to provide thickness independent selectivity. Keeping all these factors in mind, a continuous exploration for most appropriate growth precursor and inhibition layer that can be patterned at nanoscale is required. Towards this goal, for the first time, we report nano-patterning of TiO_2 using tetrakis(dimethylamido)titanium (TDMAT) *via* AS-ALD using an e-beam patterned growth inhibition polymer which has been selected among a set of polymers. At first, we present a detailed investigation to determine the efficacy of PMMA, PVP, and octafluorocyclobutane (C_4F_8) polymeric blocking layers for AS-ALD of TiO_2 harnessing TDMAT and H_2O as titanium and oxygen precursors, respectively. PMMA and PVP were deposited using spin coating and C_4F_8 was deposited using inductively coupled plasma (ICP) polymerization. Contact angle, scanning electron microscope (SEM), spectroscopic ellipsometer, and X-ray photoelectron spectroscopy (XPS) measurements were performed to determine the most compatible polymer layer for AS-ALD process of TiO_2. Finally, μm and nm-scale self-aligned growth of TiO_2 has been performed using e-beam lithography of PMMA layer. SEM, energy-dispersive X-ray spectroscopy (EDX) line scan, EDX elemental mapping, XPS line scan, and transmission electron microscope (TEM) were employed to characterize the self-aligned deposition and patterning efficiency of TiO_2.

Experimental

Materials and methods

At first, PMMA solution was prepared using 2% PMMA (Sigma-Aldrich, average M_w 350 000) in toluene while PVP solution was prepared using 1 wt% PVP (Sigma-Aldrich, average M_w 1 300 000) in ethanol. PMMA and PVP films were coated on Si(100) substrate using spin coating with a revolution per

 This journal is © The Royal Society of Chemistry 2016

Published on 01 November 2016. Downloaded by Bilkent University on 12/23/2018 6:13:57 PM.

minute (RPM) value of 4000 and acceleration of 2000 for 40 s followed by a heat treatment on hot plate for 20 minutes at 110 °C to ensure the complete removal of solvent content. PMMA and PVP film thicknesses were measured as ~43 and 60 nm, respectively utilizing spectroscopic ellipsometer. C_4F_8 layer was coated by plasma polymerization using ICP reactor (SPTS 615). Deposition of C_4F_8 was performed for 70 s using feed gas flow rate of 70 Sccm. A plasma power of 400 W was employed and deposition was carried out at room temperature. C_4F_8 layer thickness was measured as ~32 nm using spectroscopic ellipsometry. As reference control samples, Si(100) samples were solvent-cleaned and exposed to O_2 plasma for 2 minutes before TiO_2 growth in order to increase the concentration of hydroxyl groups on the substrate surface. TiO_2 was deposited using TDMAT and H_2O as titanium and oxygen precursors, respectively with N_2 as carrier gas. ALD experiments were carried out at 150 °C in Savannah S100 ALD reactor (Cambridge Nanotech Inc.). One unit growth cycle of TiO_2 consisted of TDMAT pulse (0.03 s), N_2 purge (20 s), H_2O pulse (0.015 s), and N_2 purge (20 s).

Film characterization and patterning

Contact angle of metal oxides and substrates have been obtained using static contact angle measurement setup (OCA 30). A water droplet of 4 µL has been dropped on the samples surface to measure the contact angle. Film thicknesses have been determined using a variable angle spectroscopic ellipsometer (V-VASE, J.A. Woollam Co. Inc., Lincoln, NE) which is coupled with rotating analyzer and xenon light source. The ellipsometric spectra were collected at three angles of incidence (65°, 70°, and 75°) to yield adequate sensitivity over the full spectral range. Film thickness values were extracted by fitting the spectroscopic ellipsometer data using Cauchy model, while substrate was taken as default Si(100) in V-Vase Woollam software. Elemental composition, and chemical bonding states of the metal oxide thin films were obtained by XPS measurements using Thermo Scientific K-Alpha spectrometer (Thermo Fisher Scientific, Waltham, MA) with a monochromatized Al Kα X-ray source (spot size = 400 µm). All peaks in XPS survey scans are referenced to C1s peak for charge correction and quantification of survey scans have been performed using Avantage software. Surface morphologies of the TiO_2 thin films were determined using focused ion beam (FIB) scanning electron microscope (FIB system (FEI Nova 600i Nanolab)). EDX line scan was conducted using 506 points, while EDX elemental mapping was performed using 16 frames with a resolution of 1024 × 800 on patterned TiO_2 region. XPS line scan was performed on a mm-scale TiO_2 pattern using 123 points with a spot size of ~100 µm. Tecnai G2 F30 transmission electron microscope (TEM) (FEI, Hillsboro, OR) was utilized for TEM imaging of TiO_2 patterned sample. TEM sample was prepared by a Nova 600i Nanolab FIB system (FEI, Hillsboro, OR) with an acceleration voltage of 30 kV using various beam currents ranging from 50 pA to 21 nA. Damage layer was removed by FIB milling at a beam voltage of 5 kV. A field emission SEM (NOVA NANOSEM 600) equipped with a nanometer pattern generation system was used to generate e-beam patterns directly on PMMA. PMMA (E-beam resist 950, glass transition temp, T_g = 95–106 °C) was spin coated on Si with an RPM and acceleration value of 4000 and 2000, respectively followed by a hot bake at 180 °C for 90 s. The accelerating voltage and dosage were 30 kV and 99.994 µC cm^{-2}, respectively, while a beam current of 0.633 nA was employed.

Results and discussion

In order to determine the most efficient surface for nucleation and growth inhibition of TiO_2, deposition was carried out on C_4F_8, PMMA, and PVP. Contact angle, spectroscopic ellipsometer, XPS, and SEM measurements were performed to investigate the ALD-TiO_2 growth behavior. PMMA and PVP were spin coated while C_4F_8 layer was coated on Si substrates *via* ICP polymerization using C_4F_8 feed gas.

Surface morphologies of the PMMA, PVP, and C_4F_8 films grown on Si (100) were examined by AFM and shown in Fig. S1(a)–(c).† All samples revealed smooth morphologies with the following root-mean-square (Rms) surface roughness values; PMMA/Si = 0.534 nm, PVP/Si = 0.158 nm, and C_4F_8/Si = 0.212 nm. PMMA film also revealed ~5–6 nm deep pinholes at few places on the sample (inset Fig. S1(a)†). Fig. 1 shows the variation in contact angle and thickness of TiO_2 with the increase in number of growth cycles on C_4F_8, PMMA, PVP, and Si(100). As PVP is soluble in water and other polar solvents, contact angle measurements using water as a solvent would not

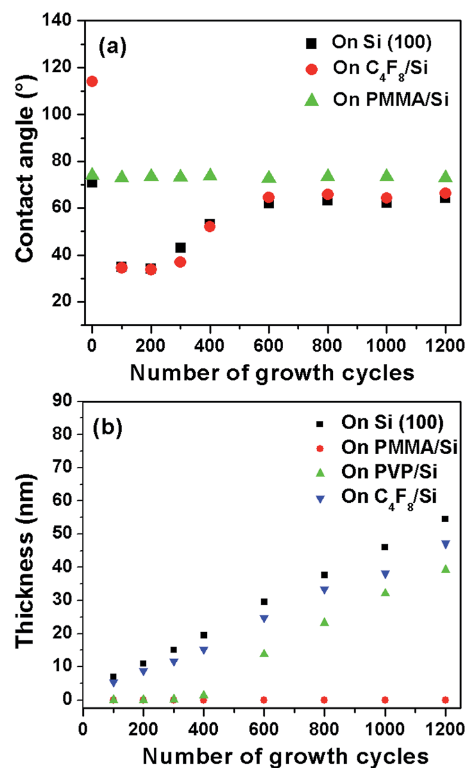

Fig. 1 Variation in (a) contact angle and (b) thickness of TiO_2 with number of growth cycles on PMMA, PVP, C_4F_8 coatings, and reference Si(100) substrate.

Published on 01 November 2016. Downloaded by Bilkent University on 12/23/2018 6:13:57 PM.

provide accurate results. Hence, contact angle measurements were only performed on C_4F_8, PMMA, and Si(100). Initial contact angle of C_4F_8, PMMA, and OH rich Si(100) was measured as 114°, 74°, and 0°, respectively. XPS analysis (Fig. S2†) showed that C_4F_8 is a mixture of fluorocarbons such as C-CF, CF, CF_2, and CF_3. The film is believed to be formed by the fragmentation of C_4F_8 monomers by plasma and dissociation of CF_x radicals.[62] Fluorocarbons are known to impart relatively high hydrophobicity to the desired surface. ICP-polymerized C_4F_8 coatings showed a contact angle of 114° which confirmed this hydrophobic nature. Contact angle of Si(100) and C_4F_8 samples reached to ~35° as soon as they were exposed to 100 cycles of TiO_2 growth. With further increase in TiO_2 growth cycles, contact angle rises again and stabilizes around ~62–63° till 1200 cycles. On the other hand, PMMA exhibits quite stable contact angle values around ~73°, almost independent of the number of TiO_2 ALD cycles. The fact that contact angle of PMMA doesn't change with TiO_2 growth cycles suggests that PMMA is efficiently blocking TiO_2 film growth. To confirm this observation, ellipsometric film thickness measurements were carried out. Fig. 1b shows the evolution of TiO_2 thickness on different surfaces as a function of ALD-growth cycles. As anticipated with conventional ALD growth processes, a linear increase in thickness of TiO_2 is observed on Si(100) with a GPC of ~0.5 Å. TiO_2 thickness increase on C_4F_8 is also linear and nearly matches with the TiO_2 growth rate on Si(100), which indicates that the initially hydrophobic plasma polymerized C_4F_8 layer is rather ineffective in blocking TiO_2 growth. On the other hand, no growth of TiO_2 is observed on PVP layers up to 300 cycles, while a very thin TiO_2 layer (~1.29 nm) is detected at 400 cycles, signaling the nucleation initiation at this growth stage on PVP coatings. With the further increase in ALD cycles beyond 400, TiO_2 eventually nucleates on PVP surface, where after the growth rate becomes similar as on Si(100).

This result suggests that PVP surface is successful in blocking/delaying the TiO_2 growth for more than 300 cycles which corresponds to an effective film thickness of ~15 nm on

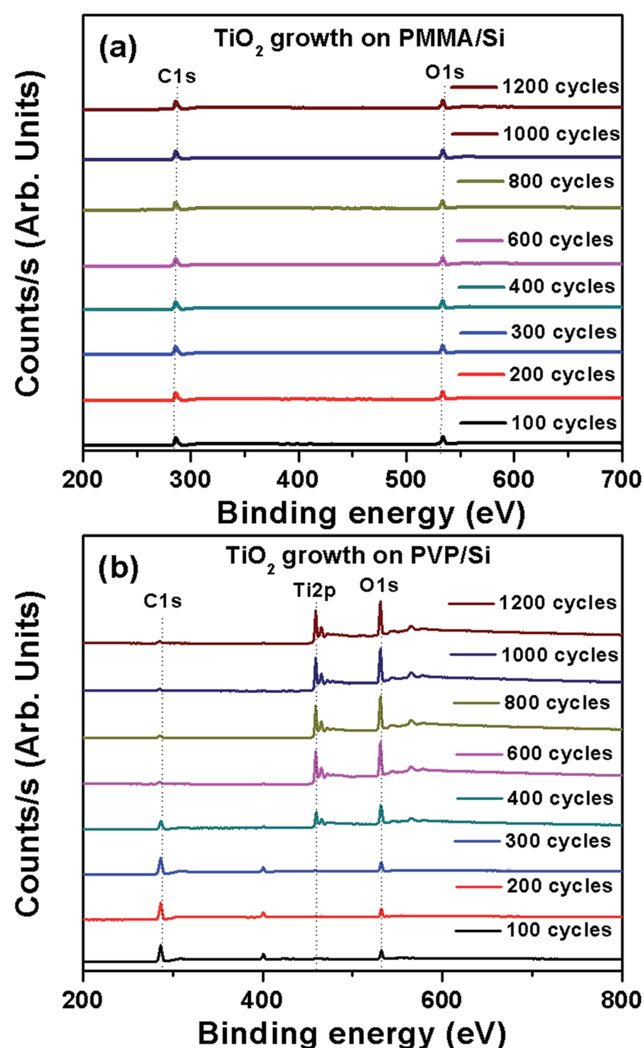

Fig. 2 XPS survey scans of TiO_2 grown with different number of ALD cycles on (a) PMMA and (b) PVP surface, confirming the effective inhibition/blocking of these layers up to more than 1200 and 300 cycles, respectively.

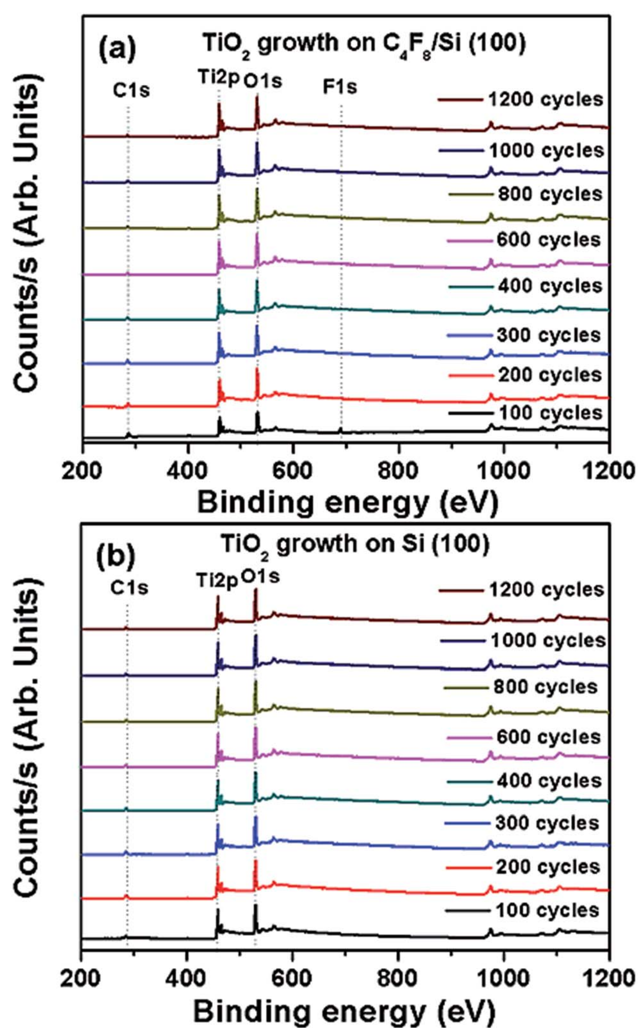

Fig. 3 XPS survey scans of TiO_2 grown with different number of ALD cycles on (a) C_4F_8/Si and (b) Si(100) revealing the presence of similar elemental composition almost independent of film growth stage, confirming a non-delayed TiO_2 deposition on both surfaces.

This journal is © The Royal Society of Chemistry 2016

Published on 01 November 2016. Downloaded by Bilkent University on 12/23/2018 6:13:57 PM.

Si surface. For PMMA-coated samples, we have observed that TiO_2 doesn't nucleate on PMMA surface at all, and no film growth is detected up to 1200 ALD cycles. These results indicate that PMMA is the most effective surface for TiO_2 growth inhibition among the coatings/surfaces studied.

Previous studies on AS-ALD established a direct correlation between surface energy and water contact angle to the growth inhibition ability of SAMs. In a case study of AS-ALD of HfO_2 with SAMs, it has been reported that only ODTS with a sufficiently high water contact angle is effective in blocking nucleation. Short or branched chained SAMs with low water contact angle were not able to inhibit nucleation of HfO_2.[63] In another study of AS-ALD of TiO_2 with mixed SAM surfaces, it was observed that extent of nucleation increases with decreasing surface energy or water contact angle of SAM surfaces.[64] Higher contact angle of SAM surfaces was only possible for well-packed SAM structures and degree of packing is an important parameter in AS-ALD processes using SAMs. High degree of packing prevents the ALD precursor access to reactive sites on Si substrates while superior hydrophobicity of SAMs prohibits the chemisorption of water which in turn blocks the nucleation of desired material. On the basis of these previous studies, one would expect C_4F_8 to show the highest nucleation delay due to its hydrophobic character and initially high contact angle. However, contact angle and spectroscopic ellipsometer measurements contradicts this prediction and show that TiO_2 nucleates on C_4F_8 with relative ease, showing almost no nucleation delay. PMMA, on the other hand, with a water contact angle significantly smaller then C_4F_8, is quite effectively blocking TiO_2 growth. Therefore, these results indicate that attaining successful AS-ALD depends on mainly two critical factors: (i) polymer blocking layer should be able to provide a sufficient barrier for ALD precursors to reach active sites on the surface, (ii) undesired reactions between inhibition layer and the ALD precursors must be avoided. In order to perform elemental quantification, XPS measurements were conducted on TiO_2 grown on PMMA, PVP, Si(100), and C_4F_8 as a function of ALD cycles up to 1200. Fig. 2 shows XPS survey scans from TiO_2 grown on PMMA and PVP coatings. Only C1s and O1s peaks are detected from PMMA surface till 1200 cycles of TiO_2 growth. Absence of any Ti peak confirms that PMMA successfully abstain itself from TiO_2 nucleation. Only C1s and O1s peaks are detected on PVP up to 300 cycles of TiO_2 growth, where after Ti2p peak is observed. Fig. 3 shows XPS survey scans from TiO_2 grown on C_4F_8 and Si(100). C1s, Ti2p, and O1s peaks are observed from TiO_2 grown on C_4F_8/Si, while F1s peak is observed from the same substrate only with 100 cycles of TiO_2 growth. As anticipated, TiO_2 growth on Si(100) reveals the peaks of C1s, Ti2p, and O1s regardless of number of ALD cycles. These results confirm the rather quick nucleation of TiO_2 and ineffective blocking behavior of both Si and C_4F_8-coated surfaces.

Table 2 Decrease in thickness of PMMA with the increase in number of TiO_2 growth cycles

Number of TiO_2 cycles	Thickness of PMMA
0	43 nm
100	42.91
200	41.516
300	37.561
400	35.45
600	33.99
800	32.84
1000	27.40
1200	23.96

Quantification of Ti in terms of atomic percentages (at%) from survey scans from all four surfaces studied is summarized in Table 1.

These XPS survey scan results provide an excellent correlation with contact angle and ellipsometer measurements and approve the following important conclusions: (i) PMMA successfully blocks/inhibits the TiO_2 deposition for at least 1200 growth cycles, which is equivalent to a blocking film thickness of ~55 nm (ii) PVP blocks TiO_2 growth up to 300 ALD cycles and further increase in growth cycles eventually leads to nucleation of TiO_2 on PVP, (iii) C_4F_8 is unable to inhibit TiO_2 nucleation and growth, despite its higher initial contact angle.

Another important observation was the decrease in PMMA film thickness with number of TiO_2 ALD cycles, which is presented in Table 2. We had chosen the substrate temperature as 150 °C which is slightly below the glass transition temperature (T_g = 108–167 °C) of PMMA.[65] Decrease in PMMA thickness might be partly due to residual solvent removal during excessively long growth periods. In addition to inherent unreactive nature of PMMA, this slight decrease in thickness of PMMA can possibly aid in achieving a better selectivity.

Fig. 4 shows the Ti2p high resolution (HR)-XPS scans obtained from TiO_2 grown on PMMA and PVP with various

Table 1 Variation in Ti at% with the increase in number of TiO_2 ALD-growth cycles

Number of ALD cycles	Ti at% on C_4F_8/Si	Ti at% on Si(100)	Ti at% on PMMA/Si(100)	Ti at% on PVP/Si(100)
100	14.06	21.23	0	0
200	21.69	23.95	0	0.92
300	22.73	23.32	0	1.15
400	23.23	23.33	0	17.25
600	22.15	25.32	0	24.93
800	24.82	25.23	0	24.82
1000	23.58	25.21	0	23.52
1200	24.52	24.21	0	24.25

Published on 01 November 2016. Downloaded by Bilkent University on 12/23/2018 6:13:57 PM.

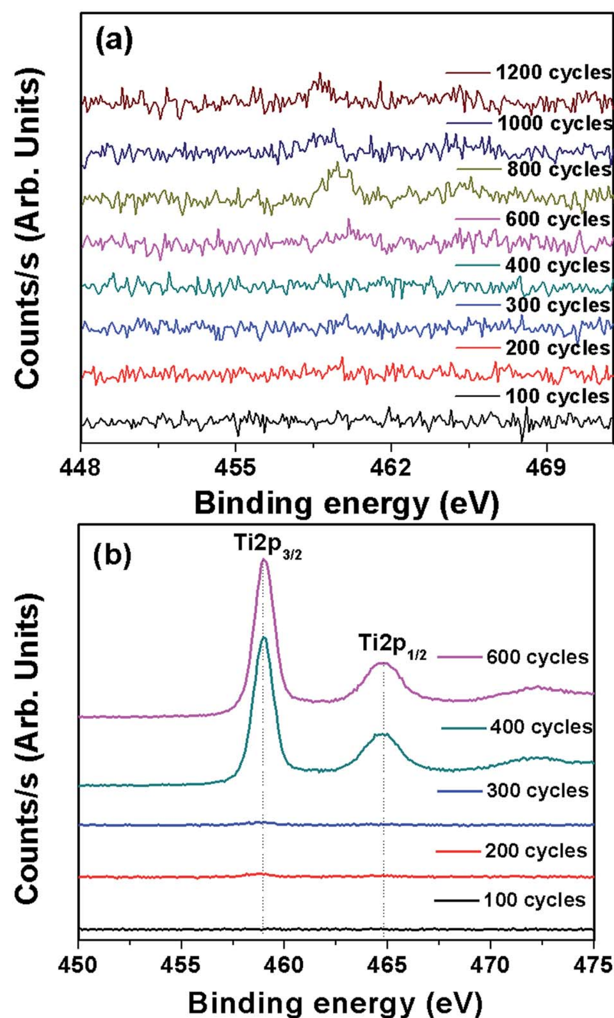

Fig. 4 HR-XPS survey scans of Ti2p obtained from TiO_2 at different stages of ALD-growth on (a) PMMA/Si(100) and (b) PVP/Si(100).

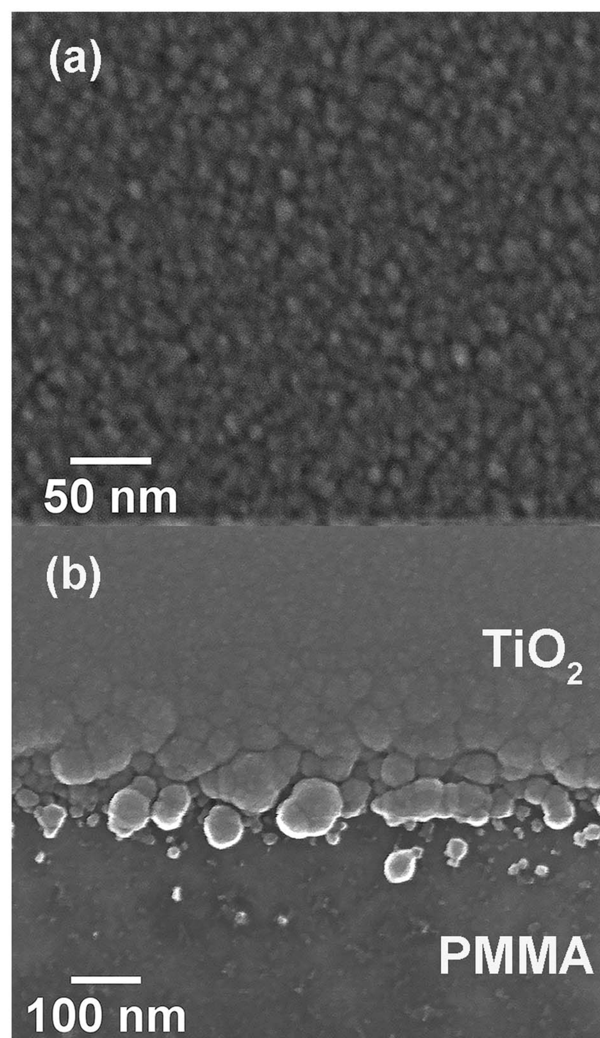

Fig. 5 SEM images of PMMA/Si surface after 1200-cycle TiO_2 growth (a) Si(100) substrate surface (b) the interface of Si(100) and PMMA showing the effective inhibition at the PMMA side.

number of ALD cycles. In accordance with the observations made by XPS survey scans, no Ti2p peak is detected from PMMA samples regardless of the number of ALD-growth cycles and on PVP up to 300 ALD cycles. $Ti2p_{3/2}$ and $Ti2p_{1/2}$ peaks are observed at a binding energy of 458.99 and 464.80 eV for 400 and 600-cycle TiO_2 respectively, grown on PVP/Si. These peaks are in agreement with the literature reports where $Ti2p_{3/2}$ and $Ti2p_{1/2}$ peaks are typically observed from TiO_2 at a binding energy value of 458.5–458.9 and 463.7–464.2 eV, respectively, which are assigned to the distinct Ti^{4+} chemical state of Ti in TiO_2.[66,67] Same Ti2p peaks are observed for PVP samples with TiO_2 ALD cycle numbers higher than 600.

SEM imaging was performed to observe the surface morphology of TiO_2 grown on Si(100) and PMMA/Si(100) after 1200 ALD cycles. During spin coating of PMMA, a part of Si substrate was deliberately covered by scotch tape, which was taken off before growth to observe the interface of TiO_2/Si and PMMA/Si. Fig. 5 reveals the surface morphology of TiO_2 (1200 growth cycles) grown on Si(100) and on the interface of TiO_2/Si-PMMA/Si. 1200-cycle TiO_2 grown on Si(100) (Fig. 5a) exhibits its grainy surface structure with 5–10 nm sized grains.

A boundary (Fig. 5b) is clearly visible at the interface of TiO_2/Si and PMMA/Si, where relatively large sized grains are observed at border on Si(100) side and PMMA surface confirms the absence of TiO_2 film growth.

Utilization of polymer films for AS-ALD studies brings an extra advantage which is their facile removal after the selective deposition process is completed. PMMA can be easily dissolved in acetone while PVP is soluble in water. After the growth of TiO_2 on PMMA with various number of growth cycles, all the samples were rinsed in acetone for 30 seconds followed by XPS measurements (Fig. 6). XPS measurements revealed the presence of O1s, C1s and Si2p peaks with the similar peak intensity from all samples after PMMA removal. Appearance of Si2p peaks from all samples makes it clear that we were successful in dissolving PMMA. It also signifies the importance of utilization of those precursors for AS-ALD processes that do not react with the polymer masking materials. Otherwise, precursors may diffuse

 This journal is © The Royal Society of Chemistry 2016

Published on 01 November 2016. Downloaded by Bilkent University on 12/23/2018 6:13:57 PM.

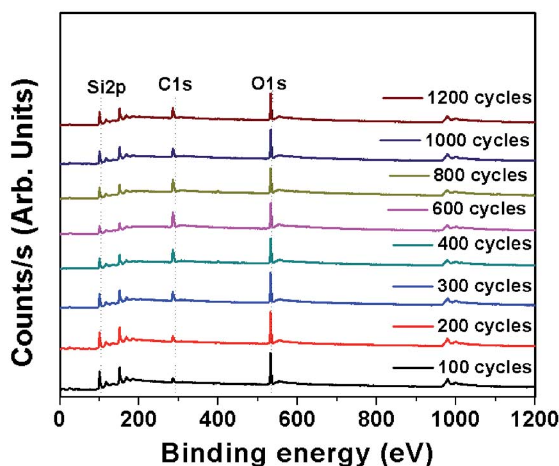

Fig. 6 XPS survey scans from sample surface after acetone treatment of PMMA layer subsequent to TiO_2 ALD cycles, confirming the facile and complete removal of polymeric blocking layer even for 1200 growth cycles at a substrate temperature of 150 °C.

into the polymer masking material and consequently making the removal of PMMA much more difficult and even not possible at all. Precursor exposure time is also very critical in avoiding the diffusion of ALD precursors into polymers and reaching the reactive sites on the substrate. In exposure mode (a trademark of Ultratech/CambridgeNanotech Inc.), dynamic vacuum was switched to static vacuum just before the precursor and oxidant pulses, and switched back to dynamic vacuum before the purging periods after waiting for some time, *i.e.*, exposure time. Time scale for precursor diffusion can be decreased by decreasing the pulse length or exposure time of precursor, however, this might result in sub-saturation precursor exposure of the surface leading to less than the optimized growth rate. We have also performed TiO_2 growth on PMMA by increasing the exposure time of TDMAT to 40 s and indeed observed film growth of TiO_2 on PMMA. In the present case, TDMAT doesn't react with PMMA within the optimized pulse length of TDMAT which makes removal of PMMA with acetone a straightforward job. We also attempted to dissolve PVP in water after TiO_2 growth, however PVP was dissolved in water up to 300 growth cycles, whereas PVP removal beyond 300 ALD cycles were not successful.

Based on contact angle, spectroscopic ellipsometer, XPS, and SEM measurements, we confidently conclude that PMMA is the most suitable blocking layer for AS-ALD of TiO_2 using TDMAT and H_2O as Ti and O precursors, respectively. Hence, we

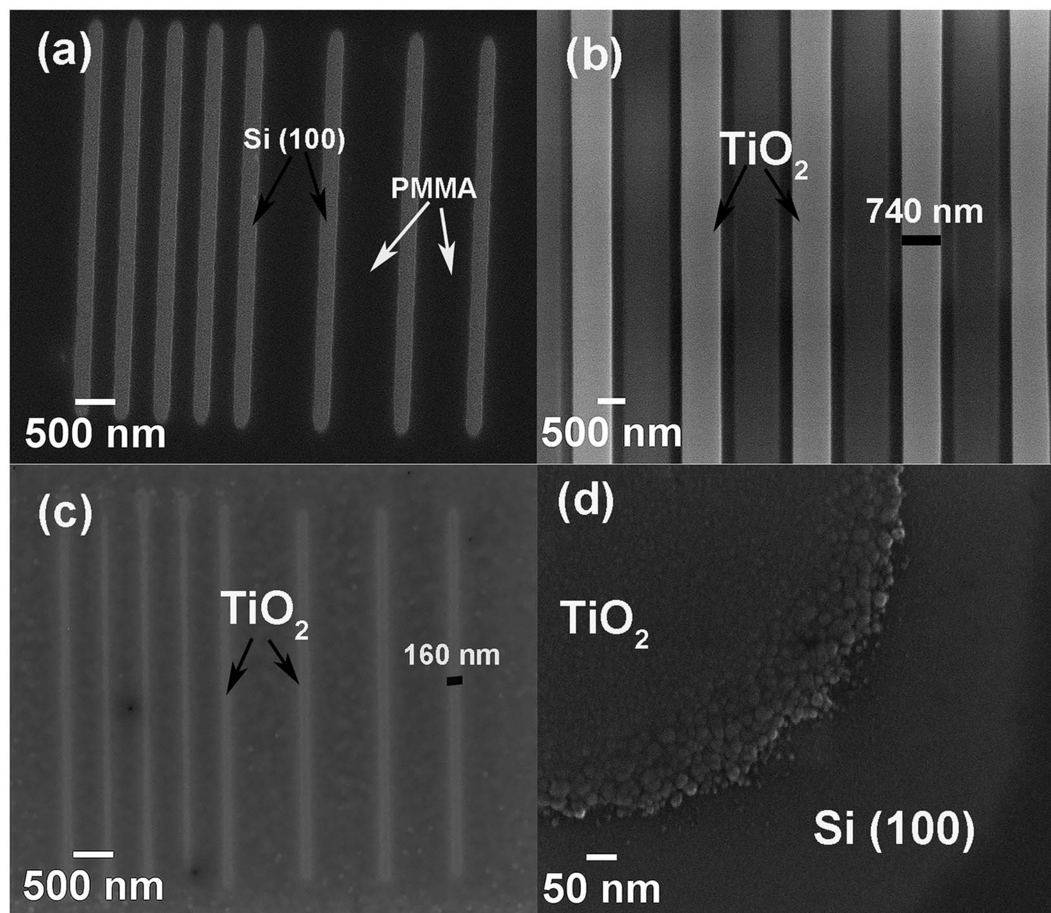

Fig. 7 SEM images of (a) e-beam exposed and post developed PMMA, (b) and (c) TiO_2 patterns grown on patterned PMMA/Si(100) surface after the removal of PMMA, (d) interface between TiO_2 pattern and Si(100).

Published on 01 November 2016. Downloaded by Bilkent University on 12/23/2018 6:13:57 PM.

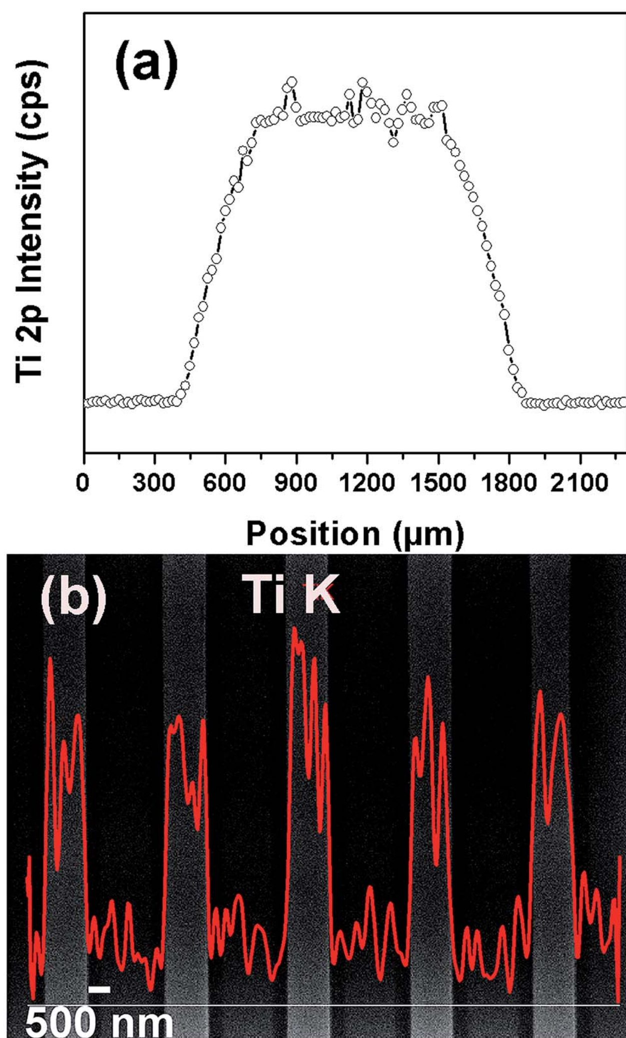

Fig. 8 (a) XPS Ti2p line scan obtained from mm-scale patterned TiO_2 grown *via* AS-ALD recipe on PMMA/Si(100) samples, (b) EDX Ti K line scan obtained from nm-scale TiO_2 line features produced *via* AS-ALD on e-beam lithography patterned samples.

selected PMMA to demonstrate the micron and sub-micron scale patterning of TiO_2 using e-beam lithography.

PMMA is by far the most commonly used e-beam lithography resist as it offers nm-scale high resolution, ease of handling, and wide process latitude. Exposure of e-beam to PMMA results in the breakage of its long chain into smaller soluble fragments, which dramatically renders it soluble in a subsequent development step. Utilization of PMMA as a common e-beam resist presents an inherent advantage to use it as a blocking layer for AS-ALD; *i.e.*, it can be patterned to produce nm scale patterns.

E-Beam lithography was performed on PMMA coated Si(100) samples to produce mm, μm, and nm scale patterns of TiO_2. Fig. 7a shows the SEM image of post-developed PMMA after exposure to e-beam revealing patterned PMMA free regions of Si. TiO_2 was grown on this e-beam exposed PMMA using 750 cycles of ALD growth at 150 °C. Samples were dipped in acetone for 30 seconds, rinsed, and dried, where after they were loaded into the SEM chamber for imaging. Fig. 7b shows the SEM

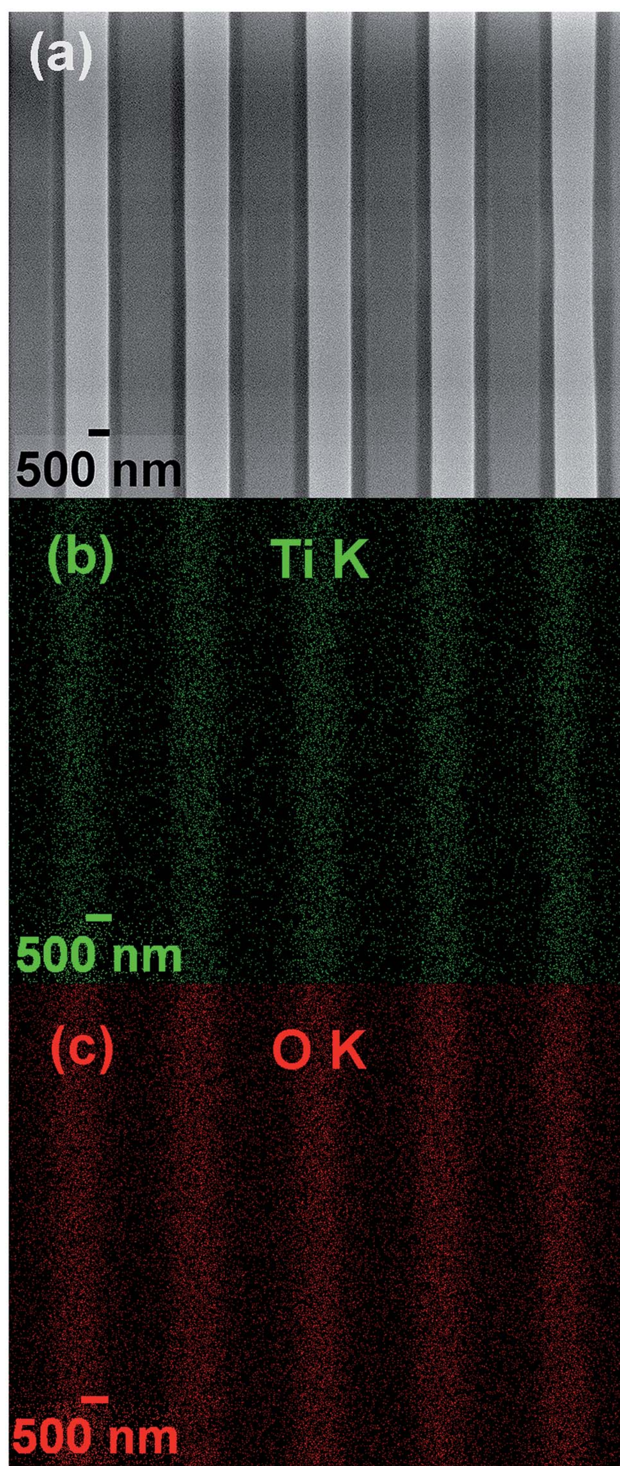

Fig. 9 SEM image of (a) TiO_2 pattern, (b) Ti K EDX elemental map, (c) O K EDX elemental map.

image of patterned TiO_2 after removal of PMMA. Growth only occurred at e-beam exposed PMMA free regions of samples and TiO_2 lines having diameter of ~740–750 nm can be clearly observed. Fig. 7c shows the TiO_2 lines prepared using the same strategy, however narrower line-widths of ~150–160 nm were produced. The debris observed between the TiO_2 lines in Fig. 7c

 This journal is © The Royal Society of Chemistry 2016

Published on 01 November 2016. Downloaded by Bilkent University on 12/23/2018 6:13:57 PM.

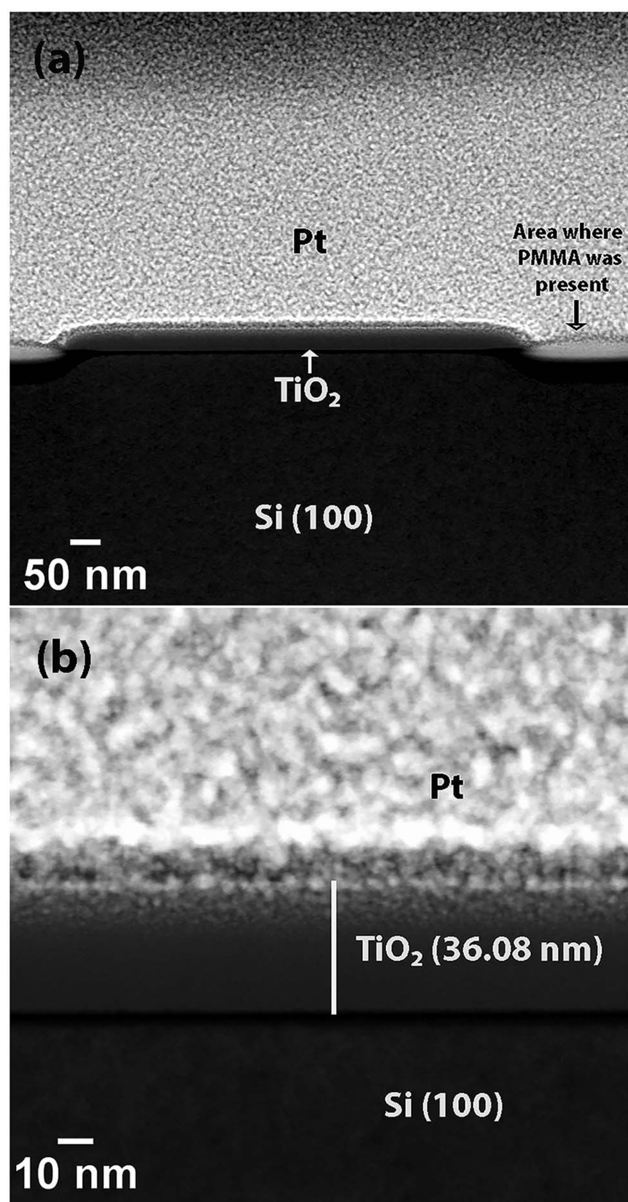

Fig. 10 TEM image of (a) TiO_2 patterned PMMA free region, (b) patterned TiO_2 region revealing the thickness uniformity of pattern.

is most probably the residue left after PMMA removal. Fig. 7d is the SEM image from the interface of the patterned TiO_2 and Si(100) revealing the grainy structure of TiO_2. Although glass transition temperature of PMMA 950 ebeam resist (95–106 °C) is less then growth temperature of TiO_2, patterning of TiO_2 is possible because of the high molecular weight of the PMMA used (950 kg mol^{-1}). The higher viscosity of the PMMA prevents reflowing to a certain extent making the patterning of TiO_2 possible.[31]

XPS and EDX elemental line scan was performed to study the linear elemental variation along the TiO_2 patterns and presented in Fig. 8. XPS line scan was performed on mm-scale TiO_2 patterns due to limitation of X-ray spot size (minimum ~ 100 μm). A line across an area of interest is selected on the sample and the XPS gathered data periodically along this line. Ti2p intensity was measured in terms of counts per second *vs.* spatial location along the line and presented in Fig. 8a. A significantly higher intensity of Ti2p peak is only observed at location of TiO_2 pattern while intensity at other points was equal to the background (noise-floor) intensity confirming the successful patterning of TiO_2. In EDX line-scanning, the electron-beam is aligned to scan across sub-micron scale features and moves along the line at a certain speed depending on the number of data points. The graph (Fig. 8b) reveals a *Y* axis modulated signal, the *Y*-height of which is an indication of the number of Ti K X-ray quanta being detected along the scan-line. Clearly, intensity of Ti K X-ray quanta increases only in TiO_2 lines which reaffirms the successful patterning of TiO_2 line structures. EDX elemental mapping is performed to determine the positions of Ti and O elements at a specific TiO_2 patterned area of the sample. X-ray elemental mapping is a useful technique where elements such as Ti and O emitting characteristic X-rays within the inspection area can be indicated by a unique color. After counting the presence of X-ray signal from a specific element, detector places a bright spot of distinct color on the screen indicating the location of that element in an area map. Such an EDX elemental map of Ti and O from a patterned TiO_2 area is provided in Fig. 9. Fig. 9a corresponds to the SEM image of patterned TiO_2 line features from which elemental maps of Ti and O are collected. Ti K and O K elemental maps are shown in Fig. 9b and c, respectively. It is evident from these elemental maps that Ti and O are only present in the line features which coincide with the TiO_2 lines shown in Fig. 9a.

Cross-sectional TEM was applied on TiO_2 patterned sample to visualize the area selective deposition. Fig. 10a and b shows the TEM images obtained after PMMA removal from a single TiO_2 pattern. Fig. 10a shows different parts of the analyzed area revealing the presence of Si, rectangular pattern of TiO_2, Pt, and the area where growth was blocked using PMMA. Fig. 10b illustrates that TiO_2 was uniformly deposited on PMMA free area with a thickness of 36.1 nm.

Conclusions

We have presented a systematic investigation on the blocking/inhibition efficacy of different polymeric materials including PMMA, PVP, and C_4F_8 for achieving selective deposition of TiO_2 *via* TDMAT and H_2O. Contact angle and spectroscopic ellipsometer measurements revealed the following results; (i) PMMA successfully blocks the TiO_2 deposition for at least 1200 ALD cycles, (ii) PVP blocks TiO_2 growth up to 300 ALD cycles, (iii) C_4F_8 is unable to inhibit TiO_2 nucleation and growth despite its initial hydrophobic character. Subsequent XPS measurements endorsed the results of contact angle and spectroscopic ellipsometer measurements as no Ti peak is observed for TiO_2 deposition up to 1200 growth cycles on PMMA-coated samples, while Ti peaks became detectable after 400 cycles on PVP and after the first 100 cycles on C_4F_8. Based on the complete TiO_2 inhibition performance on PMMA up to 1200 cycles, we conclude that PMMA is the most efficient surface to provide effective blocking of TiO_2 growth with an equivalent blocking film thickness of at least ~55 nm. SEM measurements on a 1200-cycle grown TiO_2 on Si(100) reveal the grainy structure of

Published on 01 November 2016. Downloaded by Bilkent University on 12/23/2018 6:13:57 PM.

TiO_2. We have also demonstrated that PMMA can be rather easily removed by just 30 seconds dipping into acetone solution, even after 1200 ALD-growth cycles, while PVP can be removed by dissolving in water up to 300 ALD cycles. We have demonstrated micro and nano-scale direct patterned deposition of TiO_2 using PMMA masking layer that has been patterned using e-beam lithography. SEM, EDX line scan, EDX elemental mapping, and XPS elemental mapping revealed successful patterning of μm and nm-scale TiO_2 lines. AS-ALD of TiO_2 demonstrated in the present work offers a novel approach to fabricate closely packed nanopatterns for various device architectures without any additional etching or lift-off processes.

Acknowledgements

The authors acknowledge The National Nanotechnology Research Center (UNAM), Bilkent University for providing the materials growth and characterization facilities. Authors acknowledge Mr Murat Serhatlioglu from UNAM for drawing the table of content artwork. Authors also acknowledge Dr Asli Celibioglu from UNAM for preparing PMMA and PVP solutions.

Notes and references

1 H. B. Profijt, S. E. Potts, M. C. M. Van de Sanden and W. M. M. Kessels, *J. Vac. Sci. Technol., A*, 2011, **29**, 050801.
2 R. L. Puurunen, *J. Appl. Phys.*, 2005, **97**, 121301.
3 S. M. George, *Chem. Rev.*, 2010, **110**, 111–131.
4 P. Zhang, T. S. Mayer and T. N. Jackson, *ACS Nano*, 2007, **1**, 6–9.
5 J. Goldberger, A. I. Hochbaum, R. Fan and P. Yang, *Nano Lett.*, 2006, **6**, 973–977.
6 A. J. M. Mackus, S. A. F. Dielissen, J. J. L. Mulders and W. M. M. Kessels, *Nanoscale*, 2012, **4**, 4477–4480.
7 R. Chen and S. F. Bent, *Adv. Mater.*, 2006, **18**, 1086–1090.
8 M. J. Biercuk, D. J. Monsma, C. M. Marcus, J. S. Backer and R. G. Gordon, *Appl. Phys. Lett.*, 2003, **83**, 2405–2407.
9 F. S. Minaye Hashemi, C. Prasittichai and S. F. Bent, *J. Phys. Chem. C*, 2014, **118**, 10957–10962.
10 F. S. Minaye Hashemi, C. Prasittichai and S. F. Bent, *ACS Nano*, 2015, **9**, 8710–8717.
11 A. J. M. Mackus, A. A. Bol and W. M. M. Kessels, *Nanoscale*, 2014, **6**, 10941–10960.
12 S. McDonnell, R. C. Longo, O. Seitz, J. B. Ballard, G. Mordi, D. Dick, J. H. G. Owen, J. N. Randall, J. Kim, Y. J. Chabal, K. Cho and R. M. Wallace, *J. Phys. Chem. C*, 2013, **117**, 20250–20259.
13 J. Huang, M. Lee and J. Kim, *J. Vac. Sci. Technol., A*, 2012, **30**, 01A128.
14 R. Gupta and B. G. Willis, *Appl. Phys. Lett.*, 2007, **90**, 253102.
15 A. J. M. Mackus, J. J. L. Mulders, M. C. M. Van de Sanden and W. M. M. Kessels, *J. Appl. Phys.*, 2010, **107**, 116102.
16 A. J. M. Mackus, N. F. W. Thissen, J. J. L. Mulders, P. H. F. Trompenaars, M. A. Verheijen, A. A. Bol and W. M. M. Kessels, *J. Phys. Chem. C*, 2013, **117**, 10788–10798.
17 E. Färm, S. Lindroos, M. Ritala and M. Leskelä, *Chem. Mater.*, 2012, **24**, 275–278.
18 P. R. Chalker, P. A. Marshall, K. Dawson, I. F. Brunell, C. J. Sutcliffe and R. J. Potter, *AIP Adv.*, 2015, **5**, 017115.
19 S. E. Atanasov, B. Kalanyan and G. N. Parsons, *J. Vac. Sci. Technol., A*, 2016, **34**, 01A148.
20 B. Kalanyan, P. C. Lemaire, S. E. Atanasov, M. J. Ritz and G. N. Parsons, *Chem. Mater.*, 2016, **28**, 117–126.
21 J. R. Avila, J. D. Emery, M. J. Pellin, A. B. F. Martinson, O. K. Farha and J. T. Hupp, *ACS Appl. Mater. Interfaces*, 2016, **31**, 19853–19859.
22 X. Jiang, H. Wang, J. Qi and B. G. Willis, *J. Vac. Sci. Technol., A*, 2014, **32**, 041513.
23 J. Hong, D. W. Porter, R. Sreenivasan, P. C. McIntyre and S. F. Bent, *Langmuir*, 2007, **23**, 1160–1165.
24 E. Färm, M. Kemell, M. Ritala and M. Leskela, *J. Phys. Chem.*, 2008, **112**, 15791–15795.
25 Y. Hua, W. P. King and C. L. Henderson, *Microelectron. Eng.*, 2008, **85**, 934–936.
26 J. P. Lee and M. M. Sung, *J. Am. Chem. Soc.*, 2004, **126**, 28–29.
27 J. Liu, Y. Mao, E. Lan, D. R. Banatao, G. L. Forse, J. Lu, H. O. Blom, T. O. Yeates, B. Dunn and J. P. Chang, *J. Am. Chem. Soc.*, 2008, **130**, 16908–16913.
28 G. Gay, T. Baron, C. Agraffeil, B. Salhi, T. Chevolleau, G. Cunge, H. Grampeix, J. H. Tortai, F. Martin, E. Jalaguier and B. De Salvo, *Nanotechnology*, 2010, **21**, 435301.
29 S. F. Bent, *ACS Nano*, 2007, **1**, 10–12.
30 W. Zhang and J. R. Engstrom, *J. Vac. Sci. Technol., A*, 2016, **34**, 01A107.
31 R. H. J. Vervuurt, A. Sharma, Y. Jiao, W. E. M. M. Kessels and A. A. Bol, *Nanotechnology*, 2016, **27**, 405302.
32 F. S. M. Hashemi and S. F. Bent, *Adv. Mater. Interfaces*, 2016, 1600464, DOI: 10.1002/admi.201600464.
33 S. N. Chopra, Z. Zhang, C. Kaihlanen and J. G. Ekerdt, *Chem. Mater.*, 2016, **28**, 4928–4934.
34 L. Guo, X. Qin and F. Zaera, *ACS Appl. Mater. Interfaces*, 2016, **8**, 6293–6300.
35 E. Färm, M. Kemell, M. Ritala and M. Leskelä, *Chem. Vap. Deposition*, 2006, **12**, 415–417.
36 E. Färm, M. Kemell, M. Ritala and M. Leskelä, *Thin Solid Films*, 2008, **517**, 972–975.
37 X. Jiang, R. Chen and S. F. Bent, *Surf. Coat. Technol.*, 2007, **201**, 8799–8807.
38 S. E. K. Seo, J. W. Lee, H. M. Sung-Suh and M. M. Sung, *Chem. Mater.*, 2004, **16**, 1878–1883.
39 W. H. Kim, H. B. R. Lee, K. Heo, Y. K. Lee, T. M. Chung, C. G. Kim, S. Hong, J. Heo and H. Kim, *J. Electrochem. Soc.*, 2011, **158**, D1–D5.
40 R. Chen, H. Kim, P. C. McIntyre, D. W. Porter and S. F. Bent, *Appl. Phys. Lett.*, 2005, **86**, 191910.
41 M. H. Park, Y. J. Jang, H. M. Sung-Suh and M. M. Sung, *Langmuir*, 2004, **20**, 2257–2260.
42 W. Lee, N. P. Dasgupta, O. Trejo, J. R. Lee, J. Hwang, T. Usui and F. B. Prinz, *Langmuir*, 2010, **26**, 6845–6852.
43 W. Lee and F. B. Prinz, *J. Electrochem. Soc.*, 2009, **156**, G125–G128.
44 J. Huang, M. Lee, A. Lucero, L. Cheng and J. Kim, *J. Phys. Chem. C*, 2014, **118**, 23306–23312.

This journal is © The Royal Society of Chemistry 2016

Published on 01 November 2016. Downloaded by Bilkent University on 12/23/2018 6:13:57 PM.

45 X. Jiang and S. F. Bent, *J. Electrochem. Soc.*, 2007, **154**, D648–D656.
46 K. J. Park, J. M. Doub, T. Gougousi and G. N. Parsons, *Appl. Phys. Lett.*, 2005, **86**, 051903.
47 K. Cao, Q. Zhu, B. Shan and R. Chen, *Sci. Rep.*, 2015, **5**, 8470.
48 M. Yan, Y. Koide, J. R. Babcock, P. R. Markworth, J. A. Belot, T. J. Marks and R. P. H. Chang, *Appl. Phys. Lett.*, 2001, **79**, 1709–1711.
49 K. J. Park and G. N. Parsons, *Appl. Phys. Lett.*, 2006, **89**, 043111.
50 M. N. Mullings, H. B. R. Lee, N. Marchack, X. Jiang, Z. Chen, Y. Gorlin, K. P. Lin and S. F. Bent, *J. Electrochem. Soc.*, 2010, **157**, D600–D604.
51 E. Färm, M. Kemell, E. Santala, M. Ritala and M. Leskelä, *J. Electrochem. Soc.*, 2010, **157**, K10–K14.
52 M. Coll, A. Palau, J. C. Gonzalez-Rosillo, J. Gazquez, X. Obradors and T. Puig, *Thin Solid Films*, 2014, **553**, 7–12.
53 A. Sinha, D. W. Hess and C. L. Henderson, *J. Vac. Sci. Technol., B: Microelectron. Nanometer Struct.*, 2006, **24**, 2523–2532.
54 C. R. Ellinger and S. F. Nelson, *Chem. Mater.*, 2014, **26**, 1514–1522.
55 J. M. Kim, H. B. R. Lee, C. Lansalot, C. Dussarrat, J. Gatineau and H. Kim, *Jpn. J. Appl. Phys.*, 2010, **49**, 05FA10.
56 V. Suresh, M. S. Huang, M. P. Srinivasan, C. Guan, H. J. Fan and S. Krishnamoorthy, *J. Phys. Chem. C*, 2012, **116**, 23729–23734.
57 D. H. Levy, S. F. Nelson and D. Freeman, *J. Disp. Technol.*, 2009, **5**, 484–494.
58 M. Coll, J. Gazquez, A. Palau, M. Varela, X. Obradors and T. Puig, *Chem. Mater.*, 2012, **24**, 3732–3737.
59 A. Sinha, D. W. Hess and C. L. Henderson, *J. Electrochem. Soc.*, 2006, **153**, G465–G469.
60 E. C. Dandley, P. C. Lemaire, Z. Zhu, A. Yoon, L. Sheet and G. N. Parsons, *Adv. Mater. Interfaces*, 2015, **3**, 1500431.
61 J. R. Avila, E. J. Demarco, J. D. Emery, O. K. Farha, M. J. Pellin, J. T. Hupp and A. B. F. Martinson, *ACS Appl. Mater. Interfaces*, 2014, **6**, 11891–11898.
62 X. Li, X. Hua, L. Ling, G. S. Oehrlein, M. Barela and H. M. Anderson, *J. Vac. Sci. Technol., A*, 2002, **20**, 2052–2061.
63 R. Chen, H. Kim, P. C. McIntyre and S. F. Bent, *Chem. Mater.*, 2005, **17**, 536–544.
64 J. P. Lee, Y. J. Jang and M. M. Sung, *Adv. Funct. Mater.*, 2003, **13**, 873–876.
65 C. E. Porter and F. D. Blum, *Macromolecules*, 2002, **35**, 7448–7452.
66 H. Lin, A. K. Rumaiz, M. Schulz, D. Wang, R. Rock, C. P. Huang and S. I. Shah, *Mater. Sci. Eng., B*, 2008, **151**, 133–139.
67 J. Tian, H. Gao, H. Kong, P. Yang, W. Zhang and J. Chu, *Nanoscale Res. Lett.*, 2013, **8**, 533.